



# AMERICAN METEOROLOGICAL SOCIETY

*Journal of Climate*

## **EARLY ONLINE RELEASE**

This is a preliminary PDF of the author-produced manuscript that has been peer-reviewed and accepted for publication. Since it is being posted so soon after acceptance, it has not yet been copyedited, formatted, or processed by AMS Publications. This preliminary version of the manuscript may be downloaded, distributed, and cited, but please be aware that there will be visual differences and possibly some content differences between this version and the final published version.

The DOI for this manuscript is doi: 10.1175/JCLI-D-17-0793.1

The final published version of this manuscript will replace the preliminary version at the above DOI once it is available.

If you would like to cite this EOR in a separate work, please use the following full citation:

Kayano, M., and A. Setzer, 2018: Nearly synchronous multidecadal oscillations of surface air temperature in Punta Arenas and the Atlantic Multidecadal Oscillation index. *J. Climate*. doi:10.1175/JCLI-D-17-0793.1, in press.

© 2018 American Meteorological Society



1 Nearly synchronous multidecadal oscillations of surface air temperature in Punta Arenas  
2 and the Atlantic Multidecadal Oscillation index

3

4 Short title: Multidecadal oscillations of temperature in Punta Arenas

5

6 Mary Toshie Kayano Alberto W. Setzer

7

8 Instituto Nacional de Pesquisas Espaciais, Centro de Previsão de Tempo e Estudos

9 Climáticos, São José dos Campos, SP, Brazil

10

11 Corresponding author: Mary T. Kayano

12 Email: [mary.kayano@inpe.br](mailto:mary.kayano@inpe.br)

13

14 **KEYWORDS:** Climate variability, Teleconnection, South America, Atlantic

15 Multidecadal Oscillation

16

PRELIMINARY ACCEPTED VERSION

17 **Abstract**

18

19 The Atlantic Multidecadal Oscillation (AMO) signature in southern South America (SA)  
20 is examined using Punta Arenas (53.0 °S; 70.85 °W) surface air temperature (T-air)  
21 during the 1888-2016 period. T-air shows multidecadal oscillations with a significant  
22 positive correlation of 0.77 to the AMO index. The relations of Punta Arenas T-air time  
23 series with the AMO-related global sea surface temperature (SST) and regional  
24 circulation anomaly patterns are discussed. During the warm (cold) AMO phase, a cold  
25 (warm) center in southwestern Atlantic waters induces low-level anticyclonic (cyclonic)  
26 anomalies in the region, which together with the cyclonic (anticyclonic) anomalies in the  
27 southeastern Pacific channel the northerly (southerly) flow over southern SA. This  
28 meridional flow transports warm (cold) air from lower (higher) latitudes into Punta  
29 Arenas region. Therefore, the temperature horizontal advection at low level is the main  
30 thermodynamic process that alters Punta Arenas T-air in a multidecadal time scale. The  
31 use of a relation between a long T-air surface sensor series in southern SA with the AMO  
32 presents a novel approach in climate monitoring and modelling.

33

## 34 **1. Introduction**

35

36 Rising in greenhouse gas concentrations drives the current global warming and the  
37 associated changes in the climate system (Houghton et al. 1990). Therefore, surface air  
38 temperature (T-air) is one of the most important climate variables, not only in this context,  
39 but also due to its natural variations. Nevertheless, reliable instrumental long T-air records  
40 are few and restricted to some regions in the globe. Consequently, detailed studies on the  
41 T-air variations have been hampered for many regions, including large regions of the  
42 South American continent, where reliable surface observations in a relatively dense  
43 network are available beginning mainly in the 1950s (Garreaud et al. 2009). Thus, the  
44 few studies found in the literature on T-air variations over South America (SA) examined  
45 mostly the interannual timescale variability or trends during the last decades. Studies on  
46 T-air long-term trends over SA, in general, used extreme temperatures and were restricted  
47 to regions such as the Brazilian Amazon (Victoria et al. 1998), Venezuela and Colombia  
48 (Quintana –Gomes 1999), Argentina (Rusticucci and Barrucand 2004) and southern  
49 Brazil (Marengo and Camargo 2008; Sansigolo and Kayano 2010). Vargas and Naumann  
50 (2008) suggested that secular trends identified in the minimum and maximum  
51 temperature time series in eight station in southern South America are driven by the set  
52 of wet days. Naumann and Vargas (2017) showed that these time series contain also  
53 oscillations with periods varying from 18 to 25 years. They also showed that these  
54 periodicities vary over time, in particular during the 1950-1970 decades when higher  
55 variability predominated. In the southern high-latitudes, Zazulie et al. (2010) analyzed T-  
56 air variations in the Antarctic South Orkney/Orcadas del Sur Island station (60.7 °S; 44.7  
57 °W) and found no statistically significant trends from 1903 to 1950; however, for the  
58 remainder of the series a statistically significant warming was noticed throughout the four

59 seasons of the year. Vincent et al. (2005) analyzed the trends in daily temperature  
60 extremes during the 1960-2000 period in eight countries of SA and found a consistent  
61 positive trend for the daily minimum temperature for stations located in its west and east  
62 coasts.

63 For the interannual time-scale, the El Niño-Southern Oscillation (ENSO) is the  
64 most important coupled ocean-atmosphere mode responsible for climate variations over  
65 SA (Ropelewski and Halpert 1987; 1989; Zhou and Lau 2001). This climate linkage occurs  
66 through alterations in the Walker and Hadley cells creating an atmospheric circulation  
67 bridge between the tropical Pacific and tropical SA, or through the anomalous large-scale  
68 Rossby wavetrain patterns that connect the tropical Pacific and extratropical SA (Zhou  
69 and Lau 2001). Due to the regional surface differences, the ENSO effects on the South  
70 American T-air present seasonal and regional dependences documented in previous  
71 studies. An El Niño (a La Niña) related abnormal warming (cooling) occurs in subtropical  
72 and southeastern SA during winter, in tropical SA during summer and autumn, and in  
73 northern and western tropical SA during spring (Kiladis and Diaz 1989; Halpert and  
74 Ropelewski 1992; Grimm 2003; 2004; Grimm et al. 2007; Grimm and Zilli 2009; Kayano  
75 et al. 2017).

76 The T-air variability over SA on timescales longer than the interannual has been  
77 analyzed in the context of the multidecadal variability in the Pacific Ocean (Dettinger et  
78 al. 2001; Collins et al. 2009; Kayano et al. 2017). Dettinger et al. (2001) found that the  
79 climate indices in the Pacific Ocean describing the decadal ENSO-like atmospheric-  
80 oceanic mode (Zhang et al. 1997) and Pacific Decadal Oscillation (PDO) (Mantua et al.  
81 1997) are positively correlated with annual T-air over western tropical SA. For positive  
82 indices, they associated a warm tropical SA and a dry condition. In a similar analysis,  
83 Kayano et al. (2017) found seasonal differences of the non-ENSO T-air modes in SA. In

84 their analysis, the first winter and first autumn modes show a warming in subtropical SA  
85 due to the warm advection; the first spring, the first summer, the second winter and the  
86 second autumn modes show a warming in the tropical SA and a cooling in subtropical  
87 SA, respectively associated with the dryness and wetness in these areas. Collins et al.  
88 (2009), using T-air at 2 m above the earth's surface from the National Centers for  
89 Environmental Prediction/ National Center for Atmospheric Research (NCEP/NCAR)  
90 reanalysis found warmer winters in tropical SA during the 1976-2007 period in relation  
91 to the 1948-75 period.

92         The above studies stressed the T-air variability in SA in the context of Pacific  
93 large-scale phenomena such as ENSO, PDO and ENSO-like decadal Pacific mode. In  
94 contrast, the signature of the Atlantic Multidecadal Oscillation (AMO) on the T-air  
95 variability in SA has received little attention. Nevertheless, some few studies using  
96 millennial temperature reconstructions provided indications on the existence of the AMO  
97 signature in southern SA. In fact, Villalba et al. (1996) found a main 72-year spectral peak  
98 in the second principal component of the factor analysis of the alerce tree-ring data for  
99 the 980-1974 period in northern Patagonia. They noted that this spectral peak is close to  
100 the 65 to 70-year oscillation in T-air registered in the North Atlantic by Schlesinger and  
101 Ramankutty (1994). Villalba et al. (1996) suggested a connection between T-air in  
102 northern Patagonia and North Atlantic through changes in the sea surface temperature  
103 (SST) in the Weddell Sea, which in turn occur as a response to multidecadal changes in  
104 the Atlantic thermohaline circulation shown in a modeling study by Crowley and Kim  
105 (1993). Nowadays, the T-air 65 to 70-year oscillation found by Schlesinger and  
106 Ramankutty (1994) is called the AMO, a natural oceanic variability, whose signature is  
107 noted in SST and is related to decadal to multidecadal changes in the thermohaline  
108 circulation (Kerr 2000; Delworth and Mann 2000; Knight et al. 2006).

109 In the present analysis, the relations of the AMO and the T-air variability in  
110 southern SA are examined using an instrumental T-air record at surface level. This study  
111 was firstly motivated by a multidecadal oscillation in annual Punta Arenas T-air time  
112 series noticed in an exploratory analysis. Punta Arenas (53.0 °S; 70.85 °W), Chile, is one  
113 of the surface stations in southern Patagonia, a region south of 51 °S in SA with similar  
114 T-air variations shown in a cluster analysis (Coronato and Bisigato 1998). This station  
115 has the longest reliable monthly T-air time series in southern SA, with few missing data,  
116 and spans from the end of the nineteen century up to the present (1888-2017). The  
117 availability of such a long period time series allow us to examine low-frequency  
118 oscillations in this station. Thus, the main objective of the present analysis is to investigate  
119 observational evidence on the multidecadal time scale oscillations in Punta Arenas T-air  
120 time series and its relation to the AMO.

121 Data and methodology used in the present analysis are described in the following  
122 section. The connections of Punta Arenas T-air multidecadal variations with the AMO-  
123 related SST and atmospheric circulation anomaly patterns are discussed in Section 3.  
124 Conclusions are drawn in Section 4.

125

## 126 **2. Data and Methodology**

127

128 Punta Arenas monthly T-air unadjusted (hereinafter referred to as PA\_T-air) time series  
129 for the 1888-2016 period was obtained at <https://data.giss.nasa.gov/gistemp/stdata/>  
130 (GISTEMP Team; Hansen et al. 2010). The 1888-2016 period with PA\_T-air data  
131 availability defined it as the analysis period. We also used monthly gridded reanalyzed  
132 SST, sea level pressure (SLP), 1000 hPa and 850 hPa zonal and meridional winds and T-  
133 air. The SST data for the analysis period were obtained from the NOAA extended

134 reconstructed SST version V4 (ERSST) data at a 2° by 2° latitude-longitude resolution  
135 grid available at [www.esrl.noaa.gov/psd/data/gridded/data.noaa.ersst.v4.html](http://www.esrl.noaa.gov/psd/data/gridded/data.noaa.ersst.v4.html) (Huang et  
136 al. 2015). The COBE SST data provided by the NOAA/OAR/ESRL PSD, Boulder,  
137 Colorado, USA, from their Web site at <https://www.esrl.noaa.gov/psd/> were also used  
138 (Ishii et al. 2005). The atmospheric circulation and thermodynamic data at a 1° by 1°  
139 latitude-longitude resolution grid for the 1888-2014 period were derived from the version  
140 V2C Twentieth Century Reanalysis (20CR) Project available at  
141 [www.esrl.noaa.gov/psd/data/gridded/data.20thC\\_ReanV2c.html](http://www.esrl.noaa.gov/psd/data/gridded/data.20thC_ReanV2c.html) (Compo et al. 2011).  
142 Temperature horizontal advection at 850 hPa was calculated in each grid point for the  
143 1888-2014 period. The COBE SST data were used to test the robustness of the correlation  
144 map between PA\_T-air and the SST anomalies. SST data were used for the other analyses  
145 involving the ERSST.

146         The revised AMO index was calculated using the SST time series in the North  
147 Atlantic region limited at the equator, 70 °N, 80 °W and the Greenwich longitude and the  
148 global SST in the band between 70 °N and 70 °S. This index is defined as the de-trended  
149 SST anomalies averaged in the North Atlantic region from which the global SST averaged  
150 anomalies are removed (Trenberth and Shea 2006). This index was smoothed with a 121-  
151 month running mean filter. The monthly SST anomalies were obtained as the departures  
152 from means of the 1888-2016 period.

153         Because the long-term trends are not of interest here, the linear trends in the  
154 anomaly time series were removed by subtracting the linear least-squares trends. So,  
155 monthly de-trended SST, SLP, 1000 hPa zonal and meridional winds and T-air, and 850  
156 hPa temperature horizontal advection anomalies were calculated in each grid point. Prior  
157 to calculating the monthly de-trended PA\_T-air anomaly time series, its missing values  
158 were linearly interpolated. The climatologies and the linear trends were based on the



159 1888-2016 period for the PA\_T-air and SST, and on the 1888-2014 period for the SLP,  
160 1000 hPa zonal and meridional winds and T-air, and 850 hPa temperature horizontal  
161 advection.

162 The Morlet wavelet analysis was used to perform a spectrum analysis of the de-  
163 trended PA\_T-air anomaly time series, after Torrence and Compo's (1998) procedure.

164 As for the AMO definition, the 121-month running mean was the filter used for  
165 the PA\_T-air and the reanalyzed variables. The relation between the filtered PA\_T-air  
166 and AMO index time series was obtained through the linear simultaneous correlation  
167 calculation. Also, linear simultaneous correlation maps between filtered PA\_T-air and the  
168 other filtered variables (SLP, 1000 hPa winds, 850 hPa temperature horizontal advection)  
169 were constructed. In order to assess the statistical significance of the correlations, the  
170 Ebisuzaki (1997) test with 1,000 pairs of Fourier series with random phases of the filtered  
171 PA\_T-air time series and of the other involved time series was used. The significance was  
172 obtained in a manner similar to the bootstrap method. In the case of the correlation maps,  
173 it is common practice that absolute correlations greater than 0.6 are significant at the 90%  
174 confidence level.

175 Annual average PA\_T-air values for the 1888-2016 period were used to identify  
176 the cold and warm years in Punta Arenas. These values, ranked from 1 for the smallest  
177 value to 129 for the largest value, provided the percentile rank (R) time series varying  
178 from approximately zero to 1. The lower (20%) and upper (80%) quintiles were used to  
179 classify cold and warm years in Punta Arenas, respectively. These years were stratified  
180 in the AMO phases and are listed in Table 1. Anomaly composites of the unfiltered 1000  
181 hPa T-air, SLP and low-level wind anomalies of the cold years during the cold AMO  
182 phase, and of the warm events during the warm AMO phase were calculated. The  
183 statistical significance of the composites was assessed using the Student-t test and

184 considering the number of years in the composite as degrees of freedom. For a variable  
185  $X$  with  $n$  values and  $S$  standard deviation showing a Student-t distribution, only the  
186 means with absolute values exceeding  $t_{\alpha,(n-1)}S/\sqrt{(n-1)}$  are statistically significant  
187 (Panofsky and Brier 1968). The confidence level of 90% was used in all composites.

188

### 189 3. Results

190

#### 191 3.1. Punta Arenas T-air and AMO index

192

193 The Global Wavelet Power (GWP) of PA\_T-air time series shows a main 80-year peak,  
194 and two secondary peaks, one at 8 years and another one at 28 years (Figure 1b). All  
195 three peaks are significant at a 5% level. The 8-year peak in the GWP is due to the  
196 significant variances observed during the 1888-1920 period; and the 28-year peak is due  
197 to the significant variances during the 1888-1940 and 1970-2000 periods, and the main  
198 80-year peak is due to the significant variances during the entire period of analysis (Figure  
199 1a). For this latter peak, the significant variances are within the cone of influence, the  
200 region where the edge effects are important (Torrence and Compo 1998), and an option  
201 is to disregard this peak. However, Villalba et al. (1996) found a main 72-year spectral  
202 peak in the second principal component of the factor analysis of the alerce tree-ring T-air  
203 data for the 1980-1974 period in northern Patagonia. Although their analysis was based on  
204 locations north of Punta Arenas, the similar magnitude of the peaks give us more  
205 confidence on the existence of a multidecadal signal in PA\_T-air time series.

206 This multidecadal signal in PA\_T-air is also present when comparing the filtered  
207 PA\_T-air and AMO index time series. These time series show nearly synchronous highly  
208 correlated multidecadal fluctuations with a linear simultaneous correlation of 0.77, which

209 is statistically significant at 98% confidence level (Figure 2). The statistical significance  
210 of this correlation was tested using the Ebisuzaki (1997) method, in which 1000 pairs of  
211 Fourier series with random phases of the filtered AMO and PA\_T-air time series were  
212 obtained. The positive correlation means that Punta Arenas is anomalously warm (cold)  
213 during the warm (cold) AMO phase. This is an unexpected result by the fact that Punta  
214 Arenas is some 13,000 km away from the North Atlantic, where the largest AMO-related  
215 SST anomalies are centered. Figure 2 shows that the warm (or positive) AMO phase  
216 occurred during the 1888-1898, 1930-1960 and 1995-2016 periods and the cold (or  
217 negative) one, during the 1901-1926 and 1934-1964 periods.

218 In order to examine the AMO related global SST anomaly patterns, the maps of  
219 the unfiltered SST anomalies averaged during the warm and cold AMO phases were  
220 obtained (Figure 3). These maps show nearly reversed sign patterns and reproduce the  
221 AMO-related SST antisymmetric anomaly pattern between the North and South Atlantic  
222 sectors, previously obtained using distinct methods and areas of analysis from those used  
223 here (Enfield and Mestas-Nuñez 1999; Mestas-Nuñez and Enfield 1999; Goldenberg et  
224 al. 2001; Latif et al. 2006; Deser et al. 2010). An interesting feature is the presence of  
225 negative (positive) SST anomalies surrounding most of southern SA during warm (cold)  
226 AMO phase. This result strongly suggests that the positive relation between PA\_T-air and  
227 the AMO index can not be justified by the dominant low-level westerlies over southern  
228 SA and this aspect is further examined in the following sub-section.

229

### 230 **3.2 Multidecadal relations between Punta Arenas T-air and oceanic and** 231 **atmospheric conditions**

232

233 Coherently with the positive correlation between the PA\_T-air and AMO index time  
234 series, the correlation map for the ERSST SST shows the significant positive correlations  
235 in the Atlantic Ocean north of 5 °S, and the negative ones in the extratropical South  
236 Atlantic centered approximately at 60 °S, 30 °W and in the southeastern Pacific (Figure  
237 4a). The correlation map for the COBE SST presents a similar pattern, except for less  
238 significant negative correlations in the extratropical South Atlantic and southeastern  
239 Pacific (Figure 4b). The correlation pattern reproduces the main features noted during the  
240 warm AMO phase (Figures 3 and 4a). This result is consistent with the maps of the  
241 observed surface temperature regressed onto the AMO index previously obtained (Figure  
242 2 by Ting et al. 2011; Figure 1 by Lyu and Yu 2017). Both analyses show positive  
243 anomalies over the Punta Arenas area and the positive correlations between PA\_T-air and  
244 the SST anomalies in the North Atlantic here found are consistent with previous findings.

245 In this context the anomalously warm (cold) condition in Punta Arenas is  
246 associated with anomalously cold (warm) surface waters in southwest Atlantic and  
247 southeastern Pacific. However, this association can not be explained by the dominant low-  
248 level westerlies over southeastern Pacific and southern SA that occur throughout the year  
249 (Prohaska 1976; Barros et al. 2002). This westerly flow over an underlying cold (warm)  
250 region in the southeastern Pacific would bring cold (warm) condition into southern SA.

251 In fact, a low-level circulation pattern with a strong meridional component over  
252 southern SA replaces the low-level westerlies, as shown in the correlation map between  
253 PA\_T-air and SLP and 1000 hPa winds (Figure 5b). The interpretation is that the low-  
254 level northerly (southern) flow channels the lower (higher) latitude warm (cold) air into  
255 southern SA. This flow is part of the strong anticyclonic (cyclonic) anomalies associated  
256 with an anomalous high (low) pressure center in southwestern Atlantic and relatively  
257 weak opposite circulation and SLP anomaly patterns in southeastern Pacific (Figures 5a

258 and 5b). The anomalous high (low) pressure center is consistent with cold (warm) surface  
259 waters in southwestern Atlantic during the warm (cold) AMO phase (Figures 4 and 5a).  
260 Concordantly, the correlation map between filtered PA\_T-air and 850 hPa temperature  
261 horizontal advection shows positive correlations in eastern southern SA (Figure 6).  
262 Therefore, the warm (cold) advection from the lower (higher) latitudes is the main process  
263 that alters PA\_T-air in a multidecadal time scale.

264

### 265 **3.3 Composite analyses**

266

267 Table 1 shows the years in lower (20%) and upper (80%) quintiles of PA\_T-air, which  
268 were stratified in the AMO phases. Out of 22 years in the lower quintile, 20 occurred  
269 during the cold AMO phase. This means that 91% of the cold years in Punta Arenas  
270 occurred during the cold AMO phase. Furthermore, some of these years occurred  
271 sequentially, as for the cold period of 1905-1909 and 1969-1974, what indicates the low-  
272 frequency modulation of the PA\_T-air variations. Concerning the upper quintile, 12 out  
273 of 25 occurred during the warm AMO phase. This result indicates no predominance of  
274 the warm Punta Arenas years in relation to the AMO phases. This apparent inconsistent  
275 result is due to the occurrence of warm years during the cold AMO phase from 1893 to  
276 1923 (Figure 7). However, there is a predominance of warm years after 1923 during warm  
277 AMO phase. Recalling that the quintile analysis was based on the PA\_T-air data without  
278 any filtering process, the coherency of the upper and lower quintiles with the warm and  
279 cold AMO phases gives us more confidence on the results from the correlation analysis  
280 for filtered data.

281 In order to illustrate the coherency of the above results, composite analyses were  
282 done using unfiltered data for two cases: warm Punta Arenas during the warm AMO

283 phase and cold Punta Arenas during the cold AMO phase. Most characteristics of the SST  
284 anomaly pattern noted during the warm (cold) AMO phase are reproduced for the warm  
285 (cold) Punta Arenas composite of 1000 hPa T-air (Figures 3a, 3b, 8a and 9a). Also, the  
286 positive (negative) 1000 hPa T-air anomalies found over Punta Arenas and the north of  
287 the Antarctic Peninsula for the warm (cold) composite confirm Lyu and Yu (2017)  
288 findings for Punta Arenas. Consistent with the above analyses, for the warm (cold) Punta  
289 Arenas composite, the low-level wind anomaly patterns show anticyclonic (cyclonic)  
290 anomalies in the southwestern Atlantic and opposite sign circulation anomalies in the  
291 southeastern Pacific (Figures 8b and 9b).

292

#### 293 **4. Discussion and conclusions**

294

295 Using an instrumental surface air temperature (T-air) record in Punta Arenas (53.0 °S;  
296 70.85 °W), PA\_T-air, for the 1888-2016 period, the AMO signature in South America  
297 (SA) T-air is examined. It is worth recalling that we de-trended the data by removing the  
298 linear least-squares trend in each time series, and thus the anthropic effects are not  
299 considered in the present analysis.

300 PA\_T-air shows multidecadal oscillations which are simultaneously highly and  
301 positively correlated with the Atlantic Multidecadal Oscillation (AMO) index. This  
302 positive correlation is an unexpected result because Punta Arenas is 13,000 km away from  
303 the North Atlantic, where the AMO signature is strong (Figure 3) (Enfield et al. 2001;  
304 Goldenberg et al. 2001; Latif et al. 2006; Deser et al. 2010). PA\_T-air time series shows  
305 a main 80-year spectral peak that agrees with Villalba et al. (1996) findings using the  
306 alerce tree-ring T-air data for the 980-1974 period in northern Patagonia; they found a

307 main 72-year spectral peak in the second principal component of the factor analysis of  
308 these data.

309           This highly significant simultaneous correlation between PA\_T-air and AMO  
310 index does not imply a causal relation and means that both time series may reflect the  
311 same phenomenon. Here we examined this relation and provided observational evidence  
312 that it occurs through changes in the regional low-level circulation modulated by the  
313 AMO. The AMO-related near global sea surface temperature (SST) anomaly pattern  
314 previously found (Enfield and Mestas-Nuñez 1999; Mestas-Nuñez and Enfield 1999;  
315 Deser et al. 2010) were reproduced using the 1888-2016 data. A meridional SST anomaly  
316 pattern with positive (negative) values in the North Atlantic and opposite sign anomalies  
317 in the extratropical South Atlantic is established during the warm (cold) AMO phase  
318 (Figure 4). The anomalously cold (warm) center induces low-level anticyclonic  
319 (cyclonic) anomalies associated with an anomalously high (low) pressure system in the  
320 southwestern Atlantic (Figure 5). This center, together with the low-level cyclonic  
321 (anticyclonic) anomalies in the southeastern Pacific channels the low-level northerly  
322 (southerly) flow over southern SA, so that warm (cold) air is advected from the lower  
323 (higher) latitudes into Punta Arenas region (Figures 5 and 6). Therefore, the low-level  
324 westerlies that blow throughout the year and influence the climate in this region (Prohaska  
325 1976; Barros et al. 2002) are weakened due to a multidecadal low-level circulation  
326 background with a dominant meridional component. Thus, the temperature horizontal  
327 advection from the lower (higher) latitudes is the main thermodynamic process that alters  
328 PA\_T-air in a multidecadal time scale. Punta Arenas is one of the surface stations in  
329 southern Patagonia, a region south of 51 °S in SA with similar T-air variations shown in  
330 a cluster analysis (Coronato and Bisigato 1998). So, it is likely that the results for Punta  
331 Arenas might be extended for other stations in southern SA.

332           The analysis here showed that an unambiguous relation between PA\_T-air and  
333 the AMO occurs throughout the associated atmospheric circulation changes in the  
334 southern SA region and surrounding oceanic areas. This result strongly suggests that other  
335 local atmospheric systems, such as the South American low-level jet, the South Atlantic  
336 Convergence zone, the Antarctic Oscillation as well as the South Atlantic variability  
337 modes might also be modulated to some extent by the AMO. These aspects are out of the  
338 scope of the present analysis and will be analyzed in future studies. We acknowledge that  
339 uncertainties might exist in the reconstructed SST data and in the reanalyzed atmospheric  
340 (20CR) data used here. We tested the sensitivity of the results to the period used by  
341 recalculating the SST and 1000 hPa wind composites considering the events before and  
342 after 1950 separately. The main SST and wind anomaly patterns for the total period were  
343 reproduced for both periods (before and after 1950). In the case of cold Punta Arenas  
344 during cold AMO phase, the patterns for the period after 1950 represent better the  
345 corresponding patterns of the total period. In contrast, for the case of warm Punta Arenas  
346 during the warm AMO phase, the patterns for the period before 1950 represent better the  
347 corresponding patterns of the total period. The weaker representation of the cold (warm)  
348 Punta Arenas during cold (warm) AMO phase patterns during the period before (after)  
349 1950 is due to the smaller number of events than during the complementary period.  
350 Therefore, the number of the events in the composites is more crucial than the period of  
351 the analysis in defining the variable patterns. This test indicated that the uncertainties at  
352 the beginning of the time series did not affect our results and thus it guarantees the  
353 robustness of our results.

354           As far as we know, the relations of the T-air variations in southern SA registered  
355 in an instrumental time series and the AMO have not been discussed before. Our  
356 knowledge about these relations might be useful for climate monitoring purposes.



357 Furthermore, the results here reinforce that climate modelling studies should pay attention  
358 to the regional variations of the AMO-related variability.

359

## 360 **5. Acknowledgements**

361

362 The authors thank the two anonymous reviewers for their helpful comments and  
363 suggestions. The first author was partially supported by the Conselho Nacional de  
364 Desenvolvimento Científico e Tecnológico (CNPq) of Brazil under grant 302322/2017-  
365 5.

366

## 367 **References**

368

369 Barros, V. R., A. M. Grimm, and M. E. Doyle, 2002: Relationship between temperature  
370 and circulation in southeastern South America and its influence from El Niño and  
371 La Niña events. *J. Meteor. Soc. Japan*, **80**, 21-32.

372 Collins, J. M., R. R. Chaves, and V. S. Marques, 2009: Temperature Variability over  
373 South America. *J. Climate*, **2**, 5854-5869.

374 Compo, G. P., and Coauthors, 2011: The Twentieth Century Reanalysis Project. *Quart.*  
375 *J. Roy. Meteor. Soc.*, **137**, 1-28. doi: 10.1002/qj.776.

376 Coronato, F., and A. Bisigato, 1998: A temperature pattern classification in Patagonia.  
377 *Int. J. Climatol.*, **18**, 765-773.

378 Crosby, D.S., L.C. Breaker, and W.H. Gemmill, 1993: A proposed definition for vector  
379 correlation in geophysics: Theory and application. *J. Atmos. Oceanic Tech.*, **10**,  
380 355-367.

381 Crowley, T. L., and K.-Y. Kim, 1993: Towards development of a strategy for  
382 determining the origins of decadal-centennial scale climate variability. *Quart. Sci.*  
383 *Rev.*, **12**, 375-385.

384 Delworth, T. L., and M. E. Mann, 2000: Observed and simulated multidecadal variability  
385 in the Northern Hemisphere. *Climate Dyn.*, **16**, 661–676.

386 Deser, C., M. A. Alexander, S.-P. Xie, and A. S. Phillips, 2010: Sea surface temperature  
387 variability: patterns and mechanisms. *Ann. Rev. Marine Sci.*, **2**, 115-143.

388 Dettinger, M. D., D. S. Battisti, R. D. Garreaud, G. J. McCabe, and C. M. Bitz, 2001:  
389 Interhemispheric effects of interannual and decadal ENSO-like climate variations  
390 on the Americas. *Interhemispheric climate linkages: Present and Past Climates in*  
391 *the Americas and their Societal Effects*, V. Markgraf, Ed., Academic Press,  
392 Massachusetts, 1-16.

393 Ebisuzaki, W., 1997: A method to estimate the statistical significance of a correlation  
394 when the data are serially correlated. *J. Climate*, **10**, 2147-2153.

395 Enfield, D. B., and A. Mestas-Nuñez, 1999: Multiscale variabilities in global sea surface  
396 temperatures and their relationships with tropospheric climate patterns. *J. Climate*  
397 **12**, 2719-2733.

398 Enfield, D. B., A. M. Mestas-Nuñez, and P. J. Trimble, 2001: The Atlantic multidecadal  
399 oscillations and its relation to rainfall and river flows in the continental U.S.  
400 *Geophys. Res. Lett.*, **28**, 2077–2080, doi: 10.1029/2000GL012745.

401 Garreaud, R. D., M. Vuille, R. Compagnucci, and J. Marengo, 2009: Present-day South  
402 American climate. *Palaeogeog., Palaeoclimatol., Palaeoecol.*, **281**, 180-195, doi:  
403 10.1016/j.palaeo.2007.10.032.

404 Goldenberg, S. B, C. Landsea, A. M. Mestas-Nuñez, and W. M. Gray, 2001: The recent  
405 increase in Atlantic hurricane activity: causes and implications. *Science*, **293**, 474–  
406 479, doi: 10.1126/science.1060040.

407 Grimm, A. M., 2003: The El Niño impact on the summer monsoon in Brazil: regional  
408 processes versus remote influences. *J. Climate*, **16**, 263-280.

409 Grimm, A. M., 2004: How do La Niña events disturb the summer monsoon system in  
410 Brazil? *Climate Dyn.*, **22**, 123-138.

411 Grimm, A. M., J. Pal, and F. Giorgi, 2007: Connection between spring conditions and  
412 peak summer monsoon rainfall in South America: Role of soil moisture, surface  
413 temperature, and topography in eastern Brazil. *J. Climate*, **20**, 5929–5945.

414 Grimm, A. M., and M. T. Zilli, 2009: Interannual variability and seasonal evolution of  
415 summer monsoon rainfall in South America. *J. Climate*, **22**, 2257-2275.

416 GISTEMP Team. 2017: *GISS Surface Temperature Analysis (GISTEMP)*. NASA  
417 Goddard Institute for Space Studies. Dataset accessed 2017-08-15  
418 at <https://data.giss.nasa.gov/gistemp/>.

419 Halpert, M. S., and C. F. Ropelewski, 1992: Surface temperature patterns associated with  
420 the Southern Oscillation. *J. Climate*, **5**, 577-593.

421 Hansen, J., R. Ruedy, M. Sato, and K. Lo, 2010: Global surface temperature change, *Rev.*  
422 *Geophys.*, **48**, RG4004, doi:10.1029/2010RG000345.

423 Huang, B., and Coauthors, 2015: Extended reconstructed sea surface temperature version  
424 4 (ERSST.v4). Part I: Upgrades and intercomparisons. *J. Climate*, **28**: 911–930.  
425 doi:10.1175/JCLI-D-14-00006.1

426 Houghton, J.T., G.J. Jenkins and J.J. Ephraums (eds.), 1990: *Climate Change: The IPCC*  
427 *Scientific Assessment*. Report prepared for Intergovernmental Panel on Climate

428 Change by Working Group I. Cambridge University Press, Cambridge, Great  
429 Britain, New York, NY, USA and Melbourne, Australia 410 pp.

430 Ishii, M., A. Shouji, S. Sugimoto, and T. Matsumoto, 2005: Objective analyses of sea-  
431 surface temperature and marine meteorological variables for the 20th Century using  
432 ICOADS and the Kobe Collection. *Int. J. Climatol.*, **25**, 865-879.

433 Kayano, M. T., R. V. Andreoli, R. A. F. Souza, and S. R. Garcia, 2017: Spatio-temporal  
434 variability modes of surface air temperature in South America during 1951-2010:  
435 ENSO and non-ENSO components. *Int. J. Climatol.*, (*published online*).

436 Kerr, R. A., 2000: A North Atlantic climate pacemaker for the centuries. *Science*, **288**,  
437 1984–1986, doi: 10.1126/science.288.5473.1984.

438 Kiladis, G., and H. F. Diaz, 1989. Global climatic anomalies associated with extremes in  
439 the Southern Oscillation. *J. Climate*, **2**, 1069-1090.

440 Knight, J. R., C. K. Folland, and A. A. Scaife 2006: Climate impacts of the Atlantic  
441 multidecadal oscillation. *Geophys. Res. Lett.*, **33**, L17706, doi:  
442 10.1029/2006GL026242.

443 Latif, M., M. Collins, H. Pohlmann, and N. Keenlyside, 2006: A review of predictability  
444 studies of Atlantic sector climate on decadal time scales. *J. Climate*, **19**, 5971-5987.

445 Lyu, K., and J.-Y. Yu, 2017: Climate impacts of the Atlantic Multidecadal Oscillation  
446 simulated in the CMIP5 models: A re-evaluation based on a revised index. *Geophys.*  
447 *Res. Lett.*, **44**, 3867-3876, doi:10.1002/2017GL072681.

448 Mantua, N. J., S. R. Hare, Y. Zhang, J. M. Wallace, and R. C. Francis, 1997: A Pacific  
449 interdecadal climate oscillation with impacts on salmon production. *Bull. Amer.*  
450 *Meteor. Soc.*, **78**, 1069-1079.

451 Marengo, J. A., and C. C. Camargo, 2008: Surface air temperature trends in southern  
452 Brazil for 1960–2002. *Int. J. Climatol.*, **28**, 893–904.

453 Mestas-Nuñez, A. M., and D. B. Enfield, 1999: Rotated global modes of non-ENSO sea  
454 surface temperature variability. *J. Climate*, **12**, 2734–2746.

455 Naumann, G., and W. Vargas, 2017: Variabilidad de baja frecuencia de la persistencia de  
456 la temperatura en el sudeste de Sudamérica. *Rev. Bras. Meteor.*, **32**, 1-12.

457 Panofsky, H. A., and G. W. Brier, 1968: *Some applications of statistics to Meteorology*,  
458 Pennsylvania State University, Pennsylvania, 224p.

459 Prohaska, F. J., 1976: Climates of Central and South America. *World Survey of*  
460 *Climatology* (vol. 12). W. Schwerdtfeger, Ed., Elsevier, Amsterdam, 532 pp.

461 Quintana-Gomez, R., 1999: Trends of maximum and minimum temperature in northern  
462 South America. *J. Climate*, **12**, 2104–2112.

463 Ropelewski, C. F., and M. S. Halpert, 1987: Global and regional scale precipitation  
464 patterns associated with the El Niño/Southern Oscillation. *Mon. Wea. Rev.*, **115**,  
465 1606-1626.

466 Ropelewski, C. F., and M. S. Halpert, 1989: Precipitation patterns associated with the  
467 high index phase of the Southern Oscillation. *J. Climate*, **2**, 268-284.

468 Rusticucci, M., and M. Barrucand, 2004: Observed trends and changes in temperature  
469 extremes over Argentina. *J. Climate*, **17**, 4099–4107.

470 Sansigolo, C. A., and M. T. Kayano, 2010: Trends of seasonal maximum and minimum  
471 temperatures and precipitation in southern Brazil for the 1913-2006 period. *Theor.*  
472 *Appl. Climatol.*, **101**, 209-216, doi: 10.1007/s00704-010-0270-2.

473 Schlesinger, M. E., and N. Ramankutty, 1994: An oscillation in the global climate system  
474 of period 65–70 years. *Nature*, **367**, 723–726.

475 Ting, M., Y. Kushnir, R. Seager, and C. Li, 2011: Robust features of Atlantic multi-  
476 decadal variability and its climate impacts. *Geophys. Res. Lett.*, **38**, L17705,  
477 doi:10.1029/2011GL048712.

478 Torrence, C., and G. P. Compo 1998: A practical guide to wavelet analysis. *Bull. Amer.*  
479 *Meteor. Soc.*, **79**, 61-78.

480 Trenberth, K. E., and D. J. Shea, 2006: Atlantic hurricanes and natural variability in 2005.  
481 *Geophys. Res. Lett.*, **33**, L12704, doi: 10.1029/2006GL026894.

482 Vargas, W.M., and G. Naumann, 2008: Impacts of climatic change and low frequency  
483 variability in reference series on daily maximum and minimum temperature in  
484 southern South America. *Reg. Environ. Change*, **8**, 45–57, doi: 10.1007/s10113-  
485 007-0041-5.

486 Victoria, R. L., L. A. Martinelli, J. M. Moraes, M. V. Ballester, and A. V. Krushche, 1998:  
487 Surface air temperature variations in the Amazon region and its borders during this  
488 century. *J. Climate*, **11**, 1105–1110.

489 Villalba, R., J. A. Boninsegna, A. Lara, T. T. Veblen, F. A. Roig, J. C. Aravena, and A.  
490 Ripalta 1996: Interdecadal climatic variations in millennial temperature  
491 reconstructions from southern South America. *Climatic Variations and Forcing*  
492 *Mechanisms of the last 2000 years*. P. D. Jones, R. S. Bradley, and J. Jouzel, Eds.,  
493 NATO ASI Series (vol. 41), Springer-Verlag, Berlin Heidelberg, 161-189.

494 Vincent, L. A., and Coauthors, 2005: Observed trends in indices of daily temperature  
495 extremes in South America 1960–2000. *J. Climate*, **18**, 5011–5023.

496 Zazulie, N., M. Rusticucci, and S. Solomon, 2010: Changes in climate at high southern  
497 latitudes: A unique daily record at Orcadas spanning 1903–2008. *J. Climate*, **23**,  
498 189-196, doi: 10.1175/2009JCLI3074.1

499 Zhang, Y., J. M. Wallace, and D. S. Battisti, 1997: ENSO-like interdecadal variability. *J.*  
500 *Climate*, **10**, 1004–1020.

501 Zhou, J., and K. M. Lau, 2001: Principal modes of interannual and decadal variability of  
502 summer rainfall over South America. *Int. J. Climatol.* **21**, 1623-1644.

503

504

505 Figure Captions

506

507 Figure 1 – (a) Local wavelet power spectrum of the continuous wavelet transform of  
508 PA\_T-air normalized by  $1/\sigma^2$  ( $\sigma^2=1^\circ\text{C}^2$ ); b) Global Wavelet Power (GWP) (in  
509 variance units). The shaded contours in (a) are at normalized variances varying  
510 from 5 to 40 with interval of 5. The closed contours in (a) encompass significant  
511 variances at 95% confidence level and the region where the edge effects are  
512 important is under the U-shape curve in (a). The dashed curve in (b) is the  
513 significance at 5% level assuming a red-noise spectrum.

514 Figure 2 – Monthly filtered PA\_T-air anomaly (black line) and AMO index (red line) time  
515 series. Both filtered with a 121-month running mean filter for the 1893-2011 period.  
516 The unit is  $^\circ\text{C}$ .

517 Figure 3 – SST anomalies averaged during: a) warm AMO phase; b) cold AMO phase.  
518 The unit is  $^\circ\text{C}$ . Areas with dotted shades encompass significant values. The  
519 continuous (dashed) line encompasses positive (negative) significant anomalies at  
520 the 95% confidence level using the Student-t test for mean. The purple dot in both  
521 maps gives the location of Punta Arenas.

522 Figure 4 – Correlations between filtered PA\_T-air and filtered SST using: a) ERSST data;  
523 b) COBE data. Areas with dotted shades encompass significant values. The  
524 continuous (dashed) line encompasses positive (negative) significant values at the  
525 90% confidence level using the Ebisuzaki (1997) test for correlation. The purple  
526 dot in both maps illustrates the location of Punta Arenas.

527 Figure 5 – Correlations between filtered PA\_T-air and filtered: a) SLP; b) 1000 hPa winds.  
528 In a), the continuous (dashed) line encompasses positive (negative) significant  
529 values at the 90% confidence level using the Ebisuzaki (1997) test for correlation.



530 In b), shaded areas encompass significant vector correlation at the 90% confidence  
531 level using the Crosby et al. (1993) test for vector correlation. Arrow at the bottom  
532 illustrates the base magnitude of the correlation vector. The purple dot in both maps  
533 illustrates the location of Punta Arenas.

534 Figure 6– Correlations between filtered PA\_T-air and filtered 850 hPa temperature  
535 horizontal advection. Display is the same as in Figure 5a.

536 Figure 7 - Temporal occurrence of upper (blue) and lower (red) quintiles of the PA\_T-air  
537 indicated, respectively by 1 and -1 and the AMO index (°C) multiplied by 3 (black  
538 continuous line).

539 Figure 8 – a) Composites for warm Punta Arenas during the warm AMO phase of: a) 1000  
540 hPa T-air anomalies; b) 1000 hPa wind anomalies. In a), areas with dotted shades  
541 encompass significant values and the continuous (dashed) lines encompass positive  
542 (negative) significant values. In b), shaded areas encompass significant wind  
543 vectors. The Student-t test for mean at the 95% confidence level was used. Arrow  
544 at the bottom illustrates the base magnitude of the wind vector. The units are °C for  
545 1000 hPa T-air, and  $\text{ms}^{-1}$  for wind vector.

546 Figure 9 – a) Composites for cold Punta Arenas during the cold AMO phase of: a) 1000  
547 hPa T-air anomalies; b) 1000 hPa wind anomalies. Display is the same as in Figure  
548 8.

549

550 Table captions

551 Table 1. Cold and warm years in Punta Arenas stratified according to the AMO phases.

552

Table 1. Cold and warm years in Punta Arenas stratified according to the AMO phases.

Cold Punta Arenas during cold AMO phase	Warm Punta Arenas during warm AMO phase	Cold Punta Arenas during warm AMO phase	Warm Punta Arenas during cold AMO phase
1905, 1906, 1907, 1908, 1909, 1914, 1966, 1969, 1970, 1971, 1972, 1973, 1974, 1976, 1977, 1984, 1986, 1991, 1995	1931, 1936, 1938, 1941, 1942, 1943, 1944, 1945, 1952, 1956, 1962, 2004, 2016	2000, 2002	1893, 1894, 1895, 1896, 1901, 1904, 1912, 1916, 1917, 1919, 1920, 1921, 1922

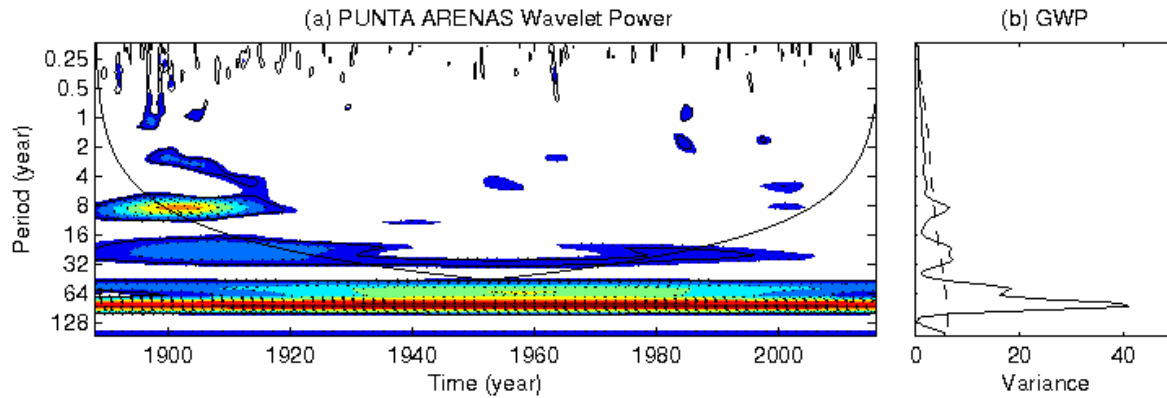


Figure 1 – (a) Local wavelet power spectrum of the continuous wavelet transform of PA\_T-air normalized by  $1/\sigma^2$  ( $\sigma^2=1^\circ\text{C}^2$ ); b) Global Wavelet Power (GWP) (in variance units). The shaded contours in (a) are at normalized variances varying from 5 to 40 with interval of 5. The closed contours in (a) encompass significant variances at 95% confidence level and the region where the edge effects are important is under the U-shape curve in (a). The dashed curve in (b) is the significance at 5% level assuming a red-noise spectrum.

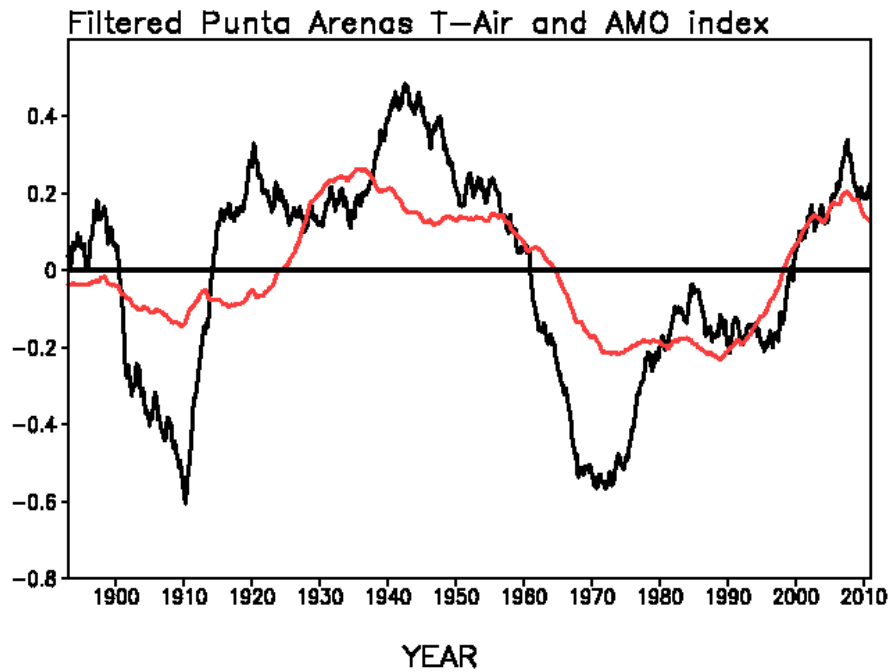


Figure 2 – Monthly filtered PA\_T-air anomaly (black line) and AMO index (red line) time series. Both filtered with a 121-month running mean filter for the 1893-2011 period. The unit is °C.

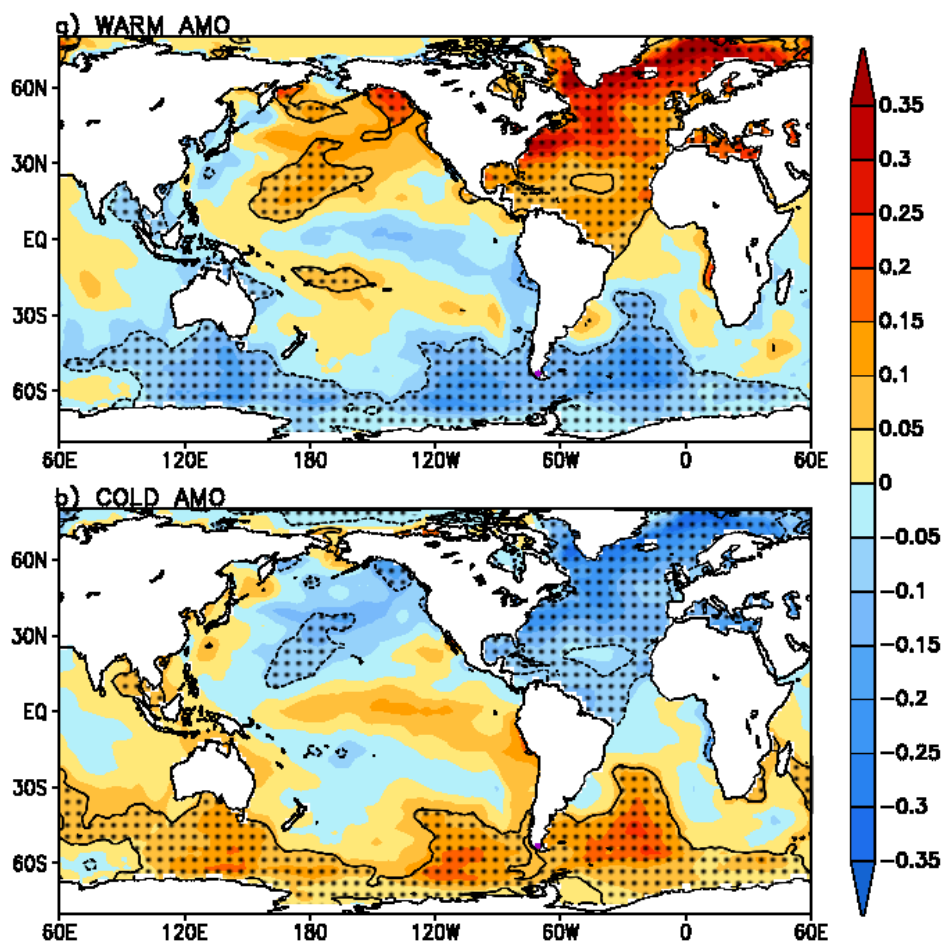


Figure 3 – SST anomalies averaged during: a) warm AMO phase; b) cold AMO phase. The unit is °C. Areas with dotted shades encompass significant values. The continuous (dashed) line encompasses positive (negative) significant anomalies at the 95% confidence level using the Student-t test for mean. The purple dot in both maps gives the location of Punta Arenas.

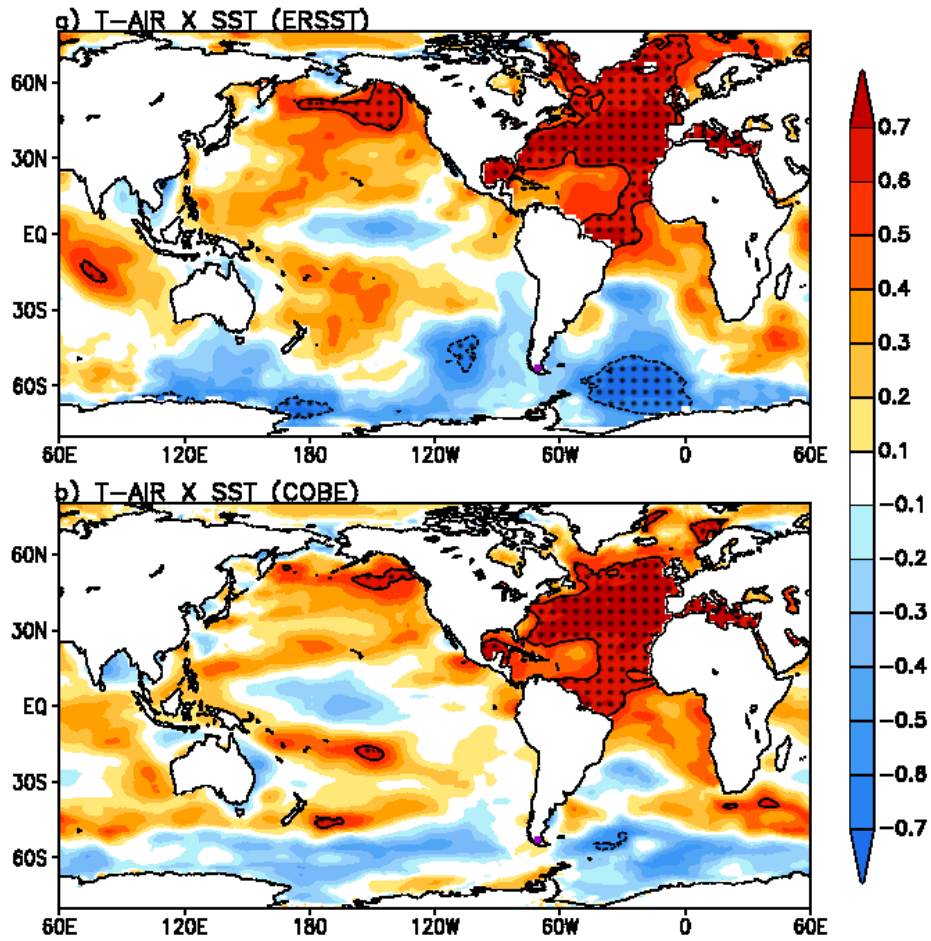


Figure 4 – Correlations between filtered PA\_T-air and filtered SST using: a) ERSST data; b) COBE data. Areas with dotted shades encompass significant values. The continuous (dashed) line encompasses positive (negative) significant values at the 90% confidence level using the Ebisuzaki (1997) test for correlation. The purple dot in both maps illustrates the location of Punta Arenas.

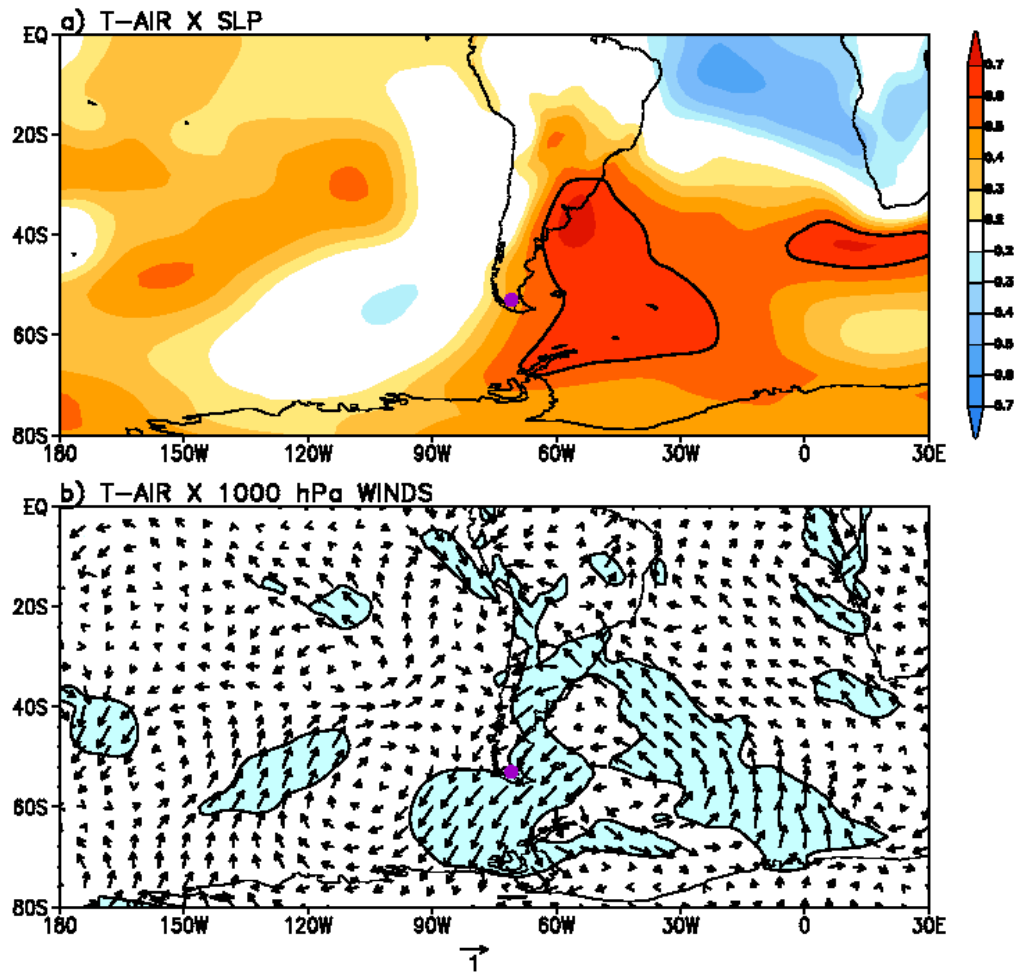


Figure 5 – Correlations between filtered PA\_T-air and filtered: a) SLP; b) 1000 hPa winds.

In a), the continuous (dashed) line encompasses positive (negative) significant values at the 90% confidence level using the Ebisuzaki (1997) test for correlation. In b), shaded areas encompass significant vector correlation at the 90% confidence level using the Crosby et al. (1993) test for vector correlation. Arrow at the bottom illustrates the base magnitude of the correlation vector. The purple dot in both maps illustrates the location of Punta Arenas.



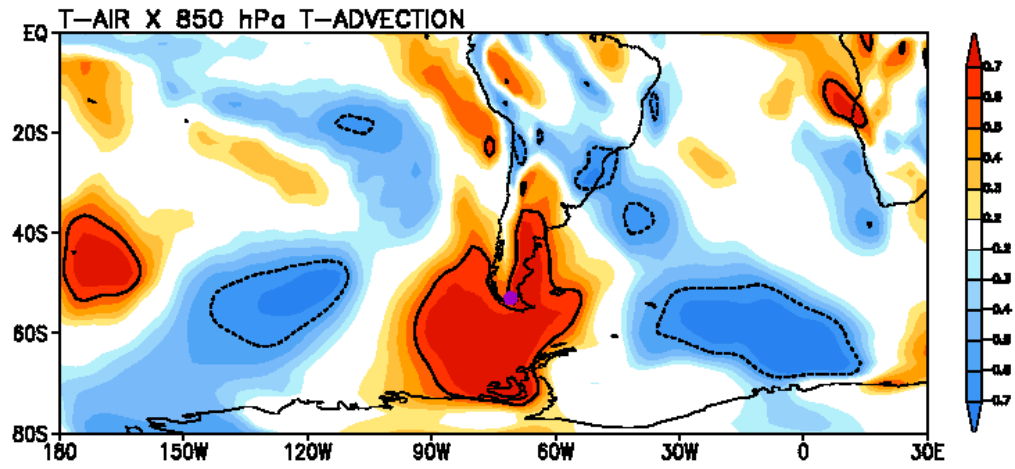


Figure 6– Correlations between filtered PA\_T-air and filtered 850 hPa temperature horizontal advection. Display is the same as in Figure 5a.

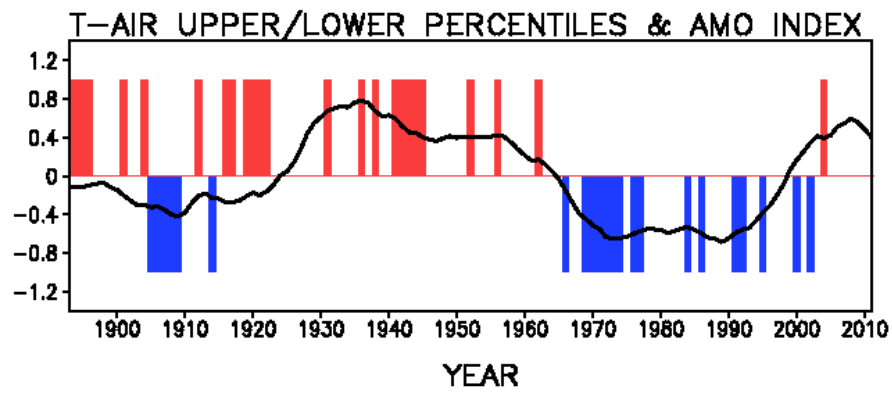


Figure 7 - Temporal occurrence of upper (blue) and lower (red) quintiles of the PA\_T-air indicated, respectively by 1 and -1 and the AMO index ( $^{\circ}\text{C}$ ) multiplied by 3 (black continuous line).

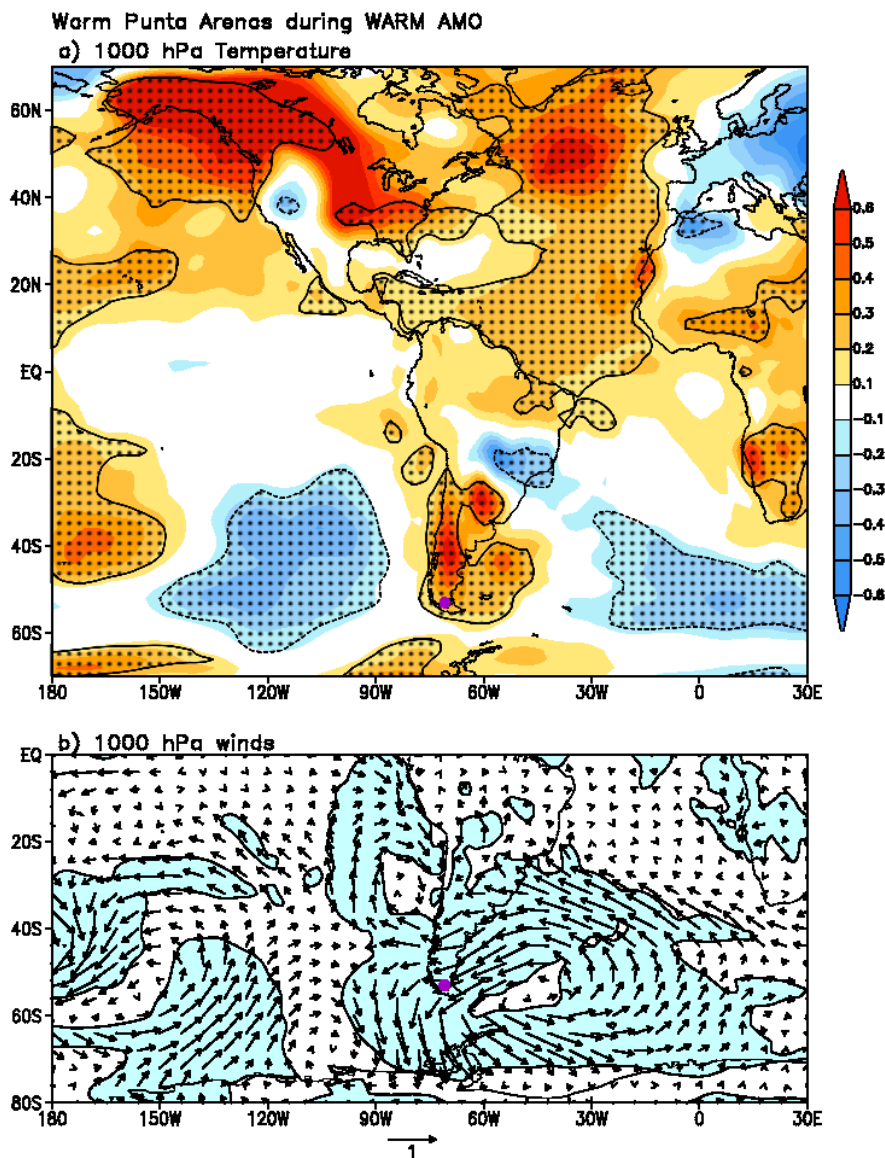


Figure 8 – a) Composites for warm Punta Arenas during the warm AMO phase of: a) 1000 hPa T-air anomalies; b) 1000 hPa wind anomalies. In a), areas with dotted shades encompass significant values and the continuous (dashed) lines encompass positive (negative) significant values. In b), shaded areas encompass significant wind vectors. The Student-t test for mean at the 90% confidence level was used. Arrow at the bottom illustrates the base magnitude of the wind vector. The units are  $^{\circ}\text{C}$  for 1000 hPa T-air, and  $\text{ms}^{-1}$  for wind vector.

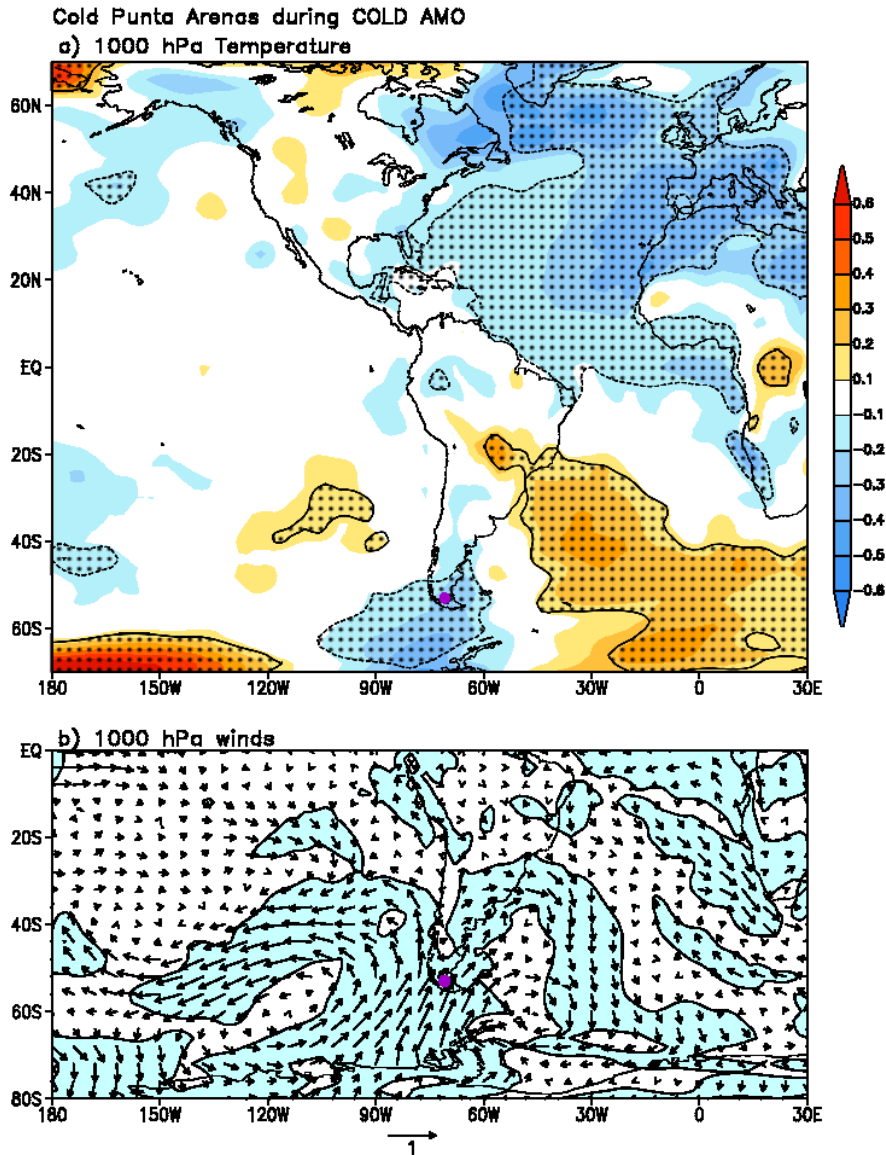


Figure 9 – a) Composites for cold Punta Arenas during the cold AMO phase of: a) 1000 hPa T-air anomalies; b) 1000 hPa wind anomalies. Display is the same as in Figure 8.